Journal of Applied Physics

Effect of Coulomb interaction on transport gap in ideal graphene nanoribbons

Cite as: J. Appl. Phys. **130**, 144301 (2021); https://doi.org/10.1063/5.0064512
Submitted: 23 July 2021 • Accepted: 17 September 2021 • Published Online: 08 October 2021

S. Ihnatsenka

Journal of Applied Physics ARTICLE scitation.org/journal/jap

Effect of Coulomb interaction on transport gap in ideal graphene nanoribbons

Cite as: J. Appl. Phys. **130**, 144301 (2021); doi: 10.1063/5.0064512
Submitted: 23 July 2021 · Accepted: 17 September 2021 ·
Published Online: 8 October 2021

S. Ihnatsenka[a)]

AFFILIATIONS

Department of Science and Technology, Linköping University, SE-60174 Norrköping, Sweden

[a)]**Author to whom correspondence should be addressed:** sergey.ignatenko@liu.se

ABSTRACT

Quantum-mechanical calculations of electron transport in ideal graphene nanoribbons show that the transport gap that is predicted by noninteracting theories vanishes if the long-range Coulomb interaction between electrons is taken into account. This is a result of charge screening with the lowest subband edge being pinned to the chemical potential. However, the transport gap reappears if a ribbon is connected to wider leads, which is typically realized in an experimental setup that is based on lithographically patterned graphene ribbons. The gap is determined by scattering at the lead-to-ribbon interface, which can already be captured by the noninteracting theory.

I. INTRODUCTION

A transport gap in graphene nanoribbons (GNRs) is defined as the range of gate voltages for which source-to-drain conductance is suppressed at zero bias.[1–4] This has been observed in all experiments on graphene nanoribbons, regardless of width, crystallographic orientation, kind of subtract, and cleanness.[1–8] Careful analysis has shown that the main reason for the transport gap is edge disorder,[8–12] which is an imperfection of an edge profile when compared to the ideal atomic arrangement of either an armchair or zigzag for a hexagonal lattice. Rough edges cause localization of electronic states inside the ribbon, and transport is consequently dominated by the hopping mechanism[3,4] or Coulomb blockade in a chain of quantum dots.[5,6] Other reasons include lattice defects and adsorbates in the bulk[7] and inhomogeneous potential due to charged impurities.[1,2,5,6] Although the strong impact of disorder on transport in GNRs has been recognized, one common feature of lithographically patterned ribbons has been overlooked—they are all connected to wide regions of graphene serving as the source and drain electrodes, and that connection might in itself cause electron scattering and thus contribute to the transport gap. One of the aims of the present study is to analyze how the interface between wide leads and a ribbon affects the transport gap.

Recent technological advances have substantially improved the quality of fabricated GNRs.[13–16] Many methods, alternative to lithography, have been demonstrated, for example, carbon nanotube and graphite unzipping,[14] organic synthesis,[15] and chemical vapor deposition on germanium.[16] Some of them allow atomic precision over ribbon width. However, the devices fabricated still suffer from various sorts of disorders: adsorbed atoms and molecules, charge puddles, ripples, etc.[13] Another issue is the connection of GNR to the metal electrode, which, in turn, suffers from the presence of a Schottky barrier,[15] the absence of covalent bonding, and interfacial contamination.[13] While all these factors affect the transport gap, it is important to understand the characteristics of an *ideal defectless* structure as a baseline.

Simple noninteracting theories based on the tight-binding calculations or the Dirac equation predict that the bandgap exists only for the armchair edge termination.[17–22] The gap is inversely proportional to the ribbon width W (disregarding the additive constant),

$$E_{gap} = \frac{\pi t a}{W}, \tag{1}$$

where $a = 0.245$ nm is the graphene lattice constant (see Fig. 1) and $t = 2.7$ eV is the hopping energy between nearest carbon atoms.[18–21] If the number of carbon dimers in the cross section of armchair GNR is[18–21]

$$N = 3p - 1, \tag{2}$$

then the gap is zero, where p is an integer and N relates to the width by $W = (N-1)a/2$. A ribbon with zero gap is referred to as metallic; otherwise, it is semiconducting. E_{gap} is the energy gap between the valence and conduction bands. This differs from the transport gap that has previously been measured in experimental setups,[1–8] where voltage is applied to a remote gate electrode to tune the charge density in the ribbon. In these setups, the ribbon and the gate form a double plate capacitor. Using the linear dispersion of graphene energy spectrum, the bandgap and the transport gap, V_{gap}, might be related as[23]

$$E_{gap} = \frac{ta}{2}\sqrt{\frac{3\pi C V_{gap}}{|e|}}, \tag{3}$$

where C is the differential capacitance, which should include the contribution from classical and quantum-mechanical capacitances.[24,25] The latter depends on quantization of the electron spectrum in the ribbon and the electron–electron interaction. As the quality of the samples improves, it is expected that the experimentally measured gaps would approach theoretically predicted values and, in particular, metallic/semiconductor alternation (2) for armchair GNRs will be confirmed. However, this has not been observed yet.

One of the reasons why the theoretical gaps, Eqs. (1) and (2), have not been observed experimentally is that they are based on the simplified theory, in which electron–electron interactions are ignored. Density functional theory calculations have shown that all GNRs possess the bandgap and that armchair GNRs, in particular, are all semiconducting.[26,27] In general, electron–electron interactions can be broken down into several components, perhaps the simplest of which is the classical Coulomb repulsion between charged particles.[28] Coulomb interactions are known to cause charge accumulation at the abrupt graphene edges.[24,25,29,30] This has been observed in capacitance measurements.[31] The main focus of this present study is the effect of the long-range Coulomb interaction on the transport gap.

Using Green's function framework, the quantum-mechanical calculations are performed in both noninteracting and interacting models with the long-range Coulomb interaction taken into account for the realistic setup where GNR is connected to wide leads, similarly to typical experiments on lithographically patterned graphene ribbons.[2–8] The main findings are as follows:

(i) The transport gap is zero in the interacting model for any ribbon width.
(ii) The gap opens up if the ribbon is connected to leads that are wider than the ribbon. The gap values reveal a faint beat pattern following semiconductor/metallic alternation for armchair GNRs, Eq. (2). However, the pattern reveals peaks instead of dips (i.e., zeros in the transport gap), which indicates higher gaps for the metallic ribbons. The gap similarly opens up for zigzag GNRs.
(iii) The inverse transport gap dependence is caused by strong electron scattering between electron states in the leads and in the ribbon, which can already be observed in the noninteracting approach.
(iv) At the conduction edge, electron interaction causes enhanced density of states along the edges of the lead-to-ribbon interface, with the current flow concentrating interior.

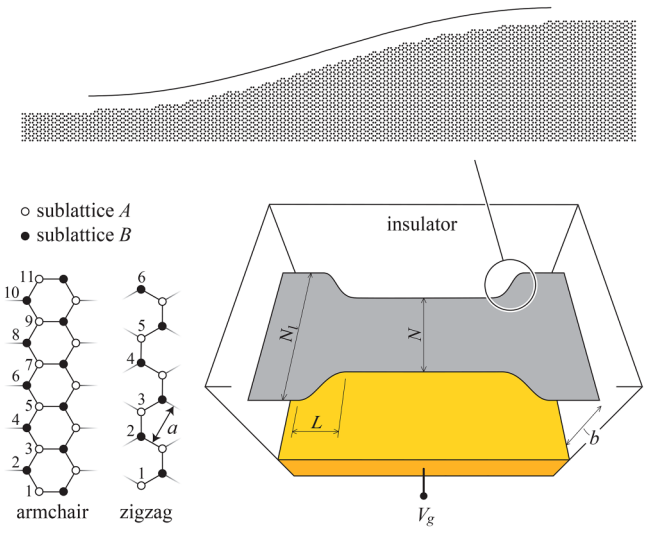

FIG. 1. Sketch of a graphene nanoribbon embedded in the insulator above the metal gate. The gate voltage V_g tunes the charge density in the ribbon connected to wider semi-infinite leads, which serve as source and drain electrodes, $N_l > N$. The leads have an armchair orientation; their width is measured in units of dimer lines. The top magnified plot shows the atomic edge profile of armchair lead-to-ribbon interface of length $L = 60$ unit cells. A mesoscopically smooth junction is profiled by a trigonometric (cosine) function. In the case of the zigzag nanoribbon, a skew applies by 30°. The left-hand side bottom plots show the unit cells of armchair $N = 11$ and zigzag $N = 6$ GNRs.

II. MODEL

The tight-binding Hamiltonian in the Hartree approximation on a honeycomb lattice is[30]

$$H = -t\sum_{\langle i,j\rangle} a_i^\dagger a_j + \sum_i V_i^H a_i^\dagger a_i, \tag{4}$$

$$V_i^H = \frac{e^2}{4\pi\varepsilon_0\varepsilon}\sum_{j\neq i} n_j\left(\frac{1}{|\mathbf{r}_i-\mathbf{r}_j|} - \frac{1}{\sqrt{|\mathbf{r}_i-\mathbf{r}_j|^2+4b^2}}\right), \tag{5}$$

where $a_i^\dagger$ is the creation operator of the electron on the site i, a_j is the destruction operator of the electron on site j, $a_i^\dagger a_i$ is the number operator, and the angle brackets denote the nearest neighbor indices. The Hartree potential V_i^H describes Coulomb interaction of electron at the ith atom with uncompensated charge density $-en$ in the system;[24,30] $-en_j$ is the electron charge at the lattice site j and $\mathbf{r}_j$ is the position vector of that site; ε is the dielectric permittivity. If the second term in (4) is omitted, then the resulting Hamiltonian becomes the standard noninteracting approximation for electrons on a graphene lattice.[22] The effects due to spin and

next-nearest-neighbor hopping are outside the scope of present study.

For the system studied here, as shown in Fig. 1, the Hartree potential is obtained by the image charges method. In this method, V^H is the sum of potentials due to the charge $-e$ and its image—fictitious charge $+e$ located inside the metal plate at distance b from the metal-to-insulator surface. Such charge arrangement satisfies the boundary condition of zero potential along the metal surface.

The observable properties of the system are obtained by the non-equilibrium Green's function framework (NEGF).[32–34] After the system is partitioned into the scattering region and two semi-infinite leads, the retarded Green's function $G^r(\mathbf{r}, \mathbf{r}', E)$ is defined as

$$\left(E - H_0(\mathbf{r}) - \Sigma_L^r(E) - \Sigma_R^r(E)\right) G^r(\mathbf{r}, \mathbf{r}', E) = \mathbf{1}, \tag{6}$$

where E is the electron energy, $\mathbf{1}$ is the unitary operator, and the retarded self-energies $\Sigma_{L/R}^r(E)$ describe coupling the scattering region with the leads. The lesser Green's function relates electron flow from right and left reservoirs into the scattering region, and by omitting the coordinate arguments reads as follows:

$$\begin{aligned} G^<(E) = &-iG^r(E)\Gamma_L(E)G^a(E)f(E-\mu_L) \\ &- iG^r(E)\Gamma_R(E)G^a(E)f(E-\mu_R), \end{aligned} \tag{7}$$

where f is the Fermi–Dirac function for the chemical potentials in the left or right lead, μ_L and μ_R, respectively, and

$$i\Gamma_{L/R}(E) = \Sigma_{L/R}^r(E) - \Sigma_{L/R}^a(E). \tag{8}$$

The surface Green's functions $\Gamma_{L/R}$ are obtained by the method given in Ref. 35.

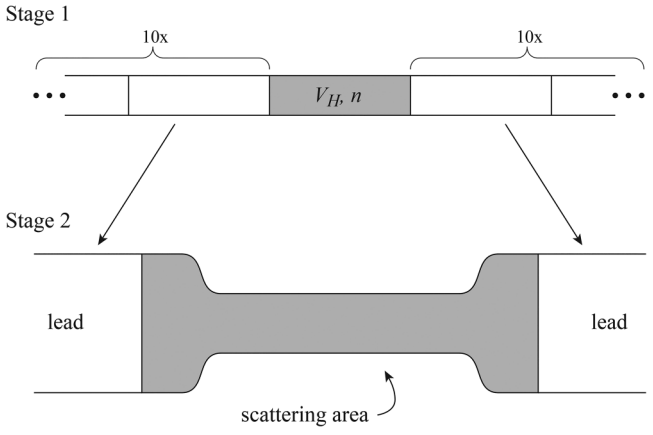

FIG. 2. Calculation stages for the Hartree potential, V_H, and charge density, n. At the first stage, the computation domain, denoted in gray, is copied ten times to the left and to the right to approximate the semi-infinite leads. V_H and n in the leads stay constant at the second stage.

The subject of this study is the transport properties of GNRs in the linear response regime. This regime falls well within the scope of the equilibrium Green's function formalism. In particular, two-terminal conductance, charge density, and local density of states are well described by the equilibrium Green's functions. However, some of the transport properties, like, for example, current, need a more detailed description, for which non-equilibrium Green's functions are used.

In equilibrium $\mu_L = \mu_R = \mu = eV_g$, the charge density is

$$n(\mathbf{r}) = \int dE\, \rho(\mathbf{r}, E) f(E-\mu), \tag{9}$$

where ρ is the local density of states expressed in terms of the retarded Green's function,

$$\rho(\mathbf{r}, E) = -\frac{1}{\pi}\mathrm{Im}[G^r(\mathbf{r}, \mathbf{r}, E)]. \tag{10}$$

The two-terminal conductance in the linear response regime is given by the Landauer formula

$$G = -\frac{2e^2}{h}\int dE\; T(E)\frac{\partial f(E-\mu)}{\partial E}, \tag{11}$$

where the transmission function follows from the Fisher–Lee relation

$$T(E) = \mathrm{Tr}[\Gamma_L(E)G^r(E)\Gamma_R(E)G^a(E)]. \tag{12}$$

To find the current density, a small bias is applied to the leads. The current flowing between two atoms in the steady state is expressed in terms of the lesser Green's function (7) as[36]

$$I_{ji} = \frac{2eti}{\hbar}\int \frac{dE}{2\pi}\left[G_{ij}^<(E) - G_{ji}^<(E)\right]. \tag{13}$$

III. METHOD

Equations (4)–(10) are solved iteratively to obtain a self-consistent solution for the charge density and Hartree potential.[30,32,33,37] To accelerate the convergence of the self-consistent calculation, the Broyden method for solving systems of nonlinear equations is used.[37] Calculation proceeds in two stages;[30] see Fig. 2. In the first stage, the self-consistent solution is achieved for the uniform computational domain, the gray area in Fig. 2, without any scattering sources. At each iteration, the Hartree potential (5) due to electrons in an infinite long ribbon needs to be obtained, which is given by the sum over j index in (5) and is the most time consuming part of the calculation. To handle the problem, in practice, the semi-infinite electron reservoirs on the left and on the right of the computational domain are replaced by finite regions of such length that any further increase does not change the results considerably. In this work, those regions are tenfold extents of the computational domain, Fig. 2, so V_H at any point is due to the direct interaction with electrons inside the computational domain and in ten times larger leads on the left and on the right. This

seemingly brute force approach is optimized by splitting the sum in (5) as

$$\sum_j \rightarrow \sum_{j\in \text{comp.domain}} + \sum_{j\in \text{leads}},$$

where the last term becomes fixed at the end of the first stage. This constitutes an assumption that the charge density in the semi-infinite leads is not affected by the scattering region. In the second stage, the scattering is imposed inside the computational domain and a self-consistent solution is achieved again. The scattering source in the present study is missing carbon atoms along the edges that shape a long narrow ribbon; see Figs. 1 and 2. Two calculation stages allow accurate accounting of the Coulomb interaction with the charges in the semi-infinite leads, and also the smooth joint between the leads and computation domain. This method differs from typical NEGF calculations,[32] where the periodic boundary condition is applied in the transport direction and, consequently, the spirituous interactions with the computational domain replica or uncompensated charges at the boundaries need to be additionally suppressed.[32,34]

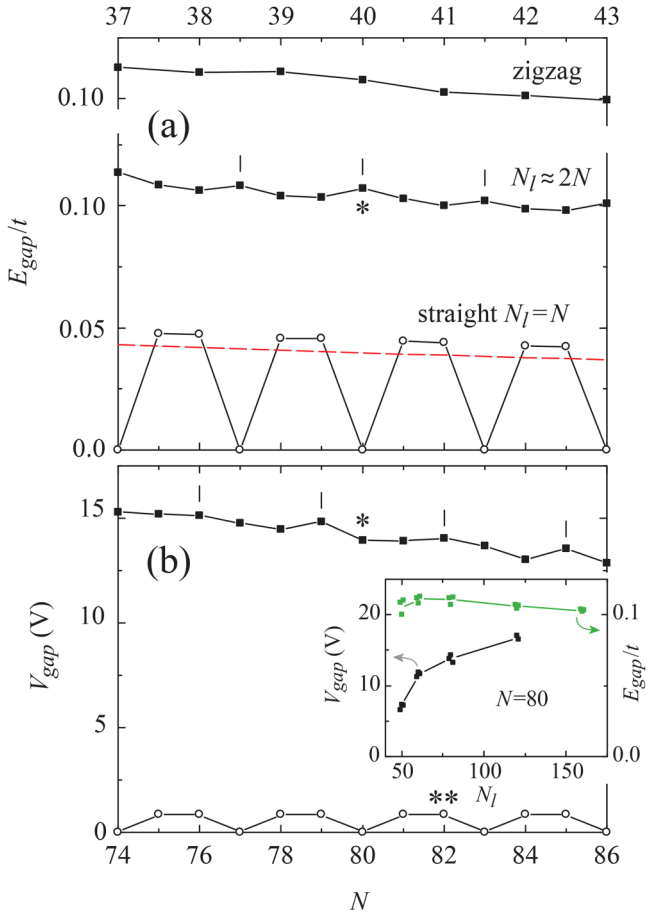

FIG. 3. Transport gap in a graphene nanoribbon in the noninteracting (a) and Hartree (b) approaches. The top part of (a) shows the result for the zigzag edge configuration, while the rest of the figure is for the armchair configuration. The lines with open circles correspond to the straight ribbons $N_l = N$, while those with filled squares correspond to geometries with wider leads. The red dashed line in (a) shows the bandgap from (1). The insert in (b) shows the gap dependence on lead width for fixed $N = 80$. The lines are given to guide the eye. The stars mark N for local density of states and current plots in Figs. 4 and 6; the double star is to link with transport gap definition in Fig. 5(a).

IV. RESULTS

The system that is studied is armchair and zigzag GNRs that are separated from the gate by SiO_2 dielectric with $\varepsilon = 3.9$ and $b = 10$ nm; see Fig. 1, which is similar to lithographically patterned GNR in experiments.[2–8] The ribbon is assumed to be ideal, and without any defects in bulk or at the edges. Its length is taken to be sufficiently large in comparison to width (2–10 times), so that the system is quasi-1D. The ribbon is connected to ideal semi-infinite leads, which are also made of graphene but of different widths, by the mesoscopically smooth junctions of length L; see Fig. 1. The leads retain the armchair orientation throughout this study. All of the edge carbon atoms are connected to two neighboring carbons and are hydrogen passivated. To eliminate any non-generic features, the results presented here are averaged over different realizations of interface length $L = 30..100$ unit cells (12..40 nm), where the one unit cell step is taken for the noninteracting calculations and ten samples in that range are chosen for the Hartree calculations. Given that atomic precision over the ribbon width is important, the width is measured in units of dimer lines for armchair GNRs and the number of carbons for zigzag GNRs; see Fig. 1. The calculations were also performed for different b and ε with similar results obtained.

To understand transport gap formation and the effect of electron–electron interaction, let us first consider the simpler noninteracting theory.

In the noninteracting theory, a straight armchair nanoribbon possesses a bandgap that doubles if the ribbon is connected to wider graphene leads (see Fig. 3); E_{gap} is additionally averaged over three neighbor lead widths $N_l = 160$, 162, and 164 (≈ 20 nm). The junction between the ribbon and leads introduces strong electron backscattering.[38–41] This can be observed as electron wave interference with minimum probability density across the junction; see Fig. 4(a). Even though the interface is mesoscopically smooth, the scattering is strong because of multiple alternations of zigzag and armchair terminations and also because of the broken graphene AB-sublattice symmetry along the edges.[40,41] A striking difference to the well-known results[18–21] is that the gap develops for any ribbon width, even for those widths that are predicted to have zero gaps for straight geometry; see Eq. (2). These metallic ribbons, in fact, reveal even slightly larger gaps, which is a result of poor matching to the zero energy state[19] of the metallic armchair ribbon extending over whole ribbon width; see Fig. 4(a). E_{gap} does not reveal dependence on the ribbon length, see Appendix A. The noninteracting theory predicts the gap for a zigzag nanoribbon to occur similarly to the armchair nanoribbon in a setup with wider leads; see Fig. 3(a). Even though the low energy states in zigzag are

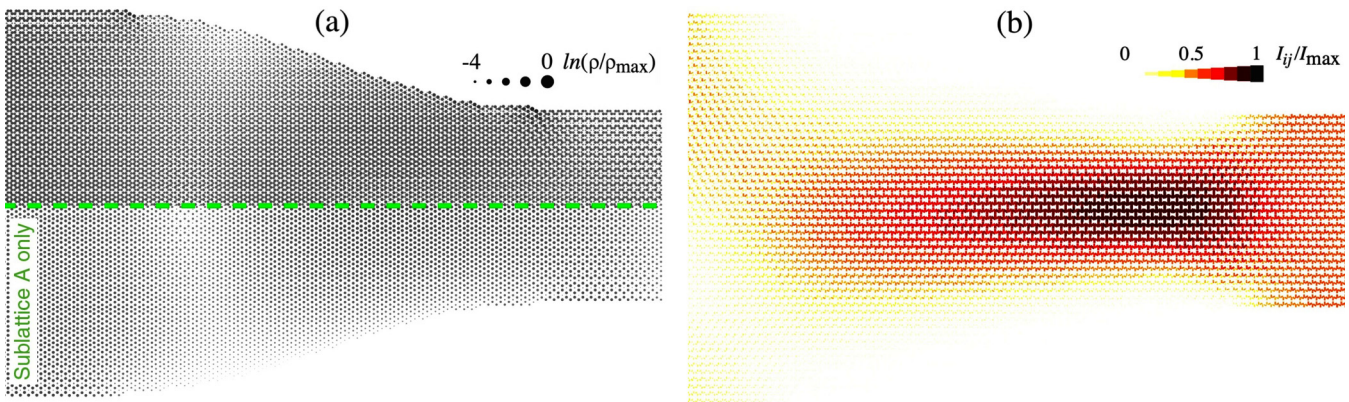

FIG. 4. Normalized local density of states (a) and current (b) in the noninteracting approach at the conduction edge. The interface between the left-hand lead and the ribbon is shown. $N = 80$ (≈ 10 nm), $N_l = 162$ (≈ 20 nm), and $L = 50$.

exponentially localized at the edges,[18] the same arguments apply for gap development as for the armchair orientation.

In contrast to the noninteracting theory, the Hartree approach predicts zero transport gap for armchair ribbons of any width having the straight geometry; see Figs. 3 and 5. This is due to the pinning[37] of the lowest subband energies to μ. The voltage applied to the back gate induces extra charges in the ribbon to establish global equilibrium. This is accompanied by the energy level shift—note that in the present calculation method, V_g is an input parameter while the charge density and electrostatic potential are allowed to vary until a self-consistent solution is obtained. For $V_g > 0$, the bottom of the conduction band aligns with μ [see Fig. 5(b)] otherwise, it is located at the top of the valence band. While the current carrying subband is at μ and $V_{gap} \approx 0$, a finite bandgap still develops, whose value corresponds to E_{gap} in noninteracting theory. Small finite V_{gap} values are still observed in Fig. 3(b) due in part to the definition adopted in this work,[42] as shown in Fig. 5(a). The Hartree calculation is carried out at $T = 100$ K, as T decreases $V_{gap} \to 0$.

The transport gap in the Hartree theory appears if a ribbon is connected to the wider leads, similarly to the noninteracting approach; see Fig. 3. The reason for the transport gap is the same for both approaches—electron backscattering at the lead-to-ribbon interface. However, in contrast to the noninteracting approach, semiconductor/metallic pattern of the armchair ribbon, Eq. (2), occurs shifted. This can be explained by an additional electrostatic potential that causes electrons to redistribute toward the edges.[24,29,30] The effect is pronounced in enhanced local density of states along the interface edges; compare Figs. 4(a) and 6(a). While electrons tend to localize at the edges, the electrical current in the Hartree approach flows more interior focused, and therefore scattering by the edge states is reduced; see Figs. 4(b) and 6(b). Another difference to the noninteracting theory is the gap dependence on the lead width N_l; see the inset in Fig. 3(b). Electrons accumulated at the interface edges mask otherwise strong scattering by small deviation from the perfectly ordered edge atomic structure.

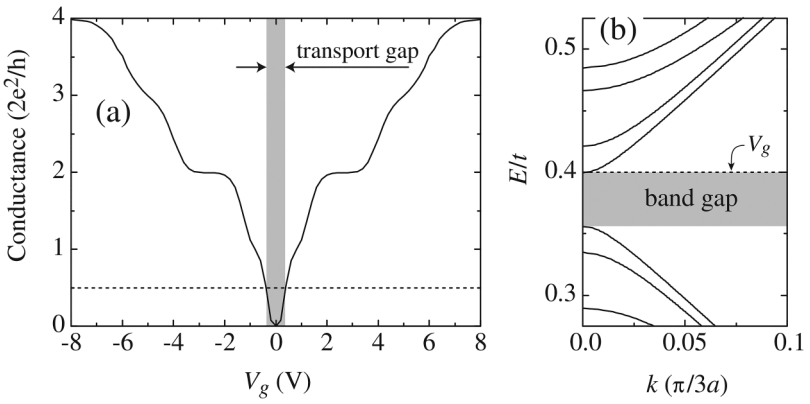

FIG. 5. Transport gap (a) and bandgap (b) in the Hartree approach. The transport gap is defined as the gate voltage range for which conductance is less than $0.5 \times 2\,e^2/h$. $V_g = 0.4$ V in (b). $N_l = N = 82$.

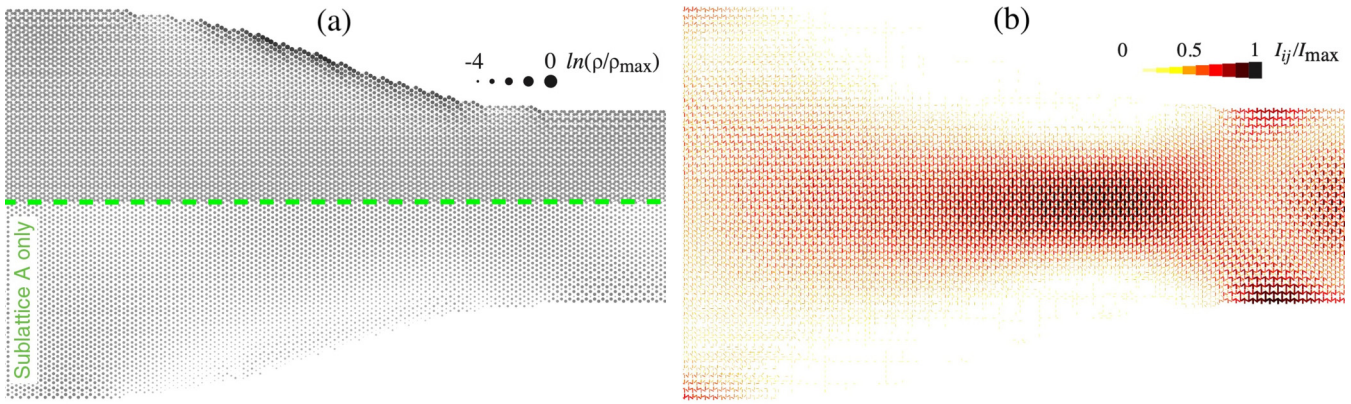

FIG. 6. (a) and (b) are the same as Figs. 4(a) and 4(b) but for the Hartree approach.

V. DISCUSSION

Graphene nanostructures are known to have intrinsically non-adiabatic transport,[39–41] which manifests in strong scattering at a wide–narrow interface and poor conductance quantization[39] in comparison, for example, to GaAs counterparts.[40] While many studies focus on the role of disorder,[9–12] which undoubtedly exists in experimental samples, the presented results demonstrate that the gap even occurs in ideal, defectless GNRs if they are connected to wide leads, which is a typical connection for lithographically patterned graphene samples.[2–8] The transport gap still follows the well-known pattern,[18–22,26] Eq. (2), but it also reflects the ability of electronic states in the leads to couple to the lowest conducting state in a ribbon. This coupling is particularly poor for the zero energy state, thus causing inverted E_{gap}-vs-N dependence; as shown in Fig. 3. This dependence is also observed in the Hartree approach, in which additional effects due to Coulomb repulsion between electrons take place.

Vanishing transport gap predicted by the Hartree approach seemingly contradicts the experimental data[1–8] measured so far. There are several reasons for this discrepancy. First, all experimental samples are contaminated by one or another form of disorder—missing carbon atoms in the lattice, adsorbed atoms and molecules, charged molecules located nearby, non-planar graphene layer, etc. Second, all lithographically patterned GNRs are connected to wider graphene regions. Third, the electronic states in the source and drain metal electrodes do not couple well with propagating states in graphene. These three factors cause strong electron backscattering and finite transport gap. The fourth reason might be the approximation itself, where classical Coulomb repulsion is taken into account but the quantum-mechanical effects of exchange and correlation interactions are not included into the theory.

The effect of energy level pinning that causes the zero transport gap in the straight GNRs is also responsible for other phenomena, such as compressible strips in the quantum Hall effect.[43,44] The alignment of the electronic states with the chemical potential (the Fermi energy) reflects the screening ability of the system when free electrons can redistribute to minimize electrostatic energy, which is a property that is peculiar to a metallic system as opposite to an insulator. Recently, the pinning of the valence band to the Fermi energy of a gold electrode has been experimentally observed in armchair GNRs.[45]

While the transport gap that is predicted in the Hartree approach is zero, the finite bandgap still exists and can be detected in optical measurements on absorption spectra.[46] Simultaneous transport and optical measurements would be of interest to study the interplay between transport and bandgaps and also to elucidate the role of electron interactions in a straight geometry. The interplay between the transport and bandgaps might also be studied in a three terminal setup, as shown in Fig. 1, where both the back gate and source-to-drain voltages vary. However, the problem of electron transport becomes more complex for finite bias because of the nonlinear screening and pinning effects.[47]

The Hartree method accounts for the classical interaction between particles, but it does not respect the principle of anti-symmetry of the wave function, which is resolved in the Hartree–Fock approach. An extension of the presented model to the Hartree–Fock model is straightforward by the addition of the exchange interaction term.[33] However, that method would require much more computational resources. The Hartree–Fock approach is able to capture Coulomb blockade physics and is thus of interest to theoretical analysis of the proposed explanation[2,5,6] of the transport gap.

One may deduce the relation between E_{gap} and V_{gap} from Fig. 3. This can be loosely related by Eq. (3), where all the effects are included in one parameter—capacitance C. It has been shown to consist of classical parallel plate capacitance and the terms due to the quantization of electron spectrum and the electron–electron interaction.[24,25] The results show that C also depends on device geometry beyond the area of parallel plates (e.g., $C \approx 0$ for straight GNR geometry). For the geometry with junction, estimations by (3) give $C = 750\,\mathrm{aF}/\mu\mathrm{m}^2$, which agree reasonably well with Ref. 3.

Measurements for the ribbon width of 25 nm reveal $V_{gap} \sim 20-30$ V.[3,6,8] These values exceed the ones obtained above, Fig. 3(b), which might be attributed to the wider width in comparison to the one explored here (10 nm), different setup geometry, and dominance by the disorder effects.

The structures considered in this study are all graphene made. In real experimental devices,[1–8] the wide graphene regions are eventually connected to the metal electrodes. That connection can modify electron transport through a GNR.[48,49] In particular, the transport gap can be suppressed due to poor coupling between states in the metal and the propagating states in the GNR, the effect that has a stronger impact on devices with small sizes.[49]

The Hartree calculation results in Ref. 24 do not reveal the pinning effect responsible for the vanishing transport gap. This might be attributed to the difference in the models: in Ref. 24, the average charge density is an input parameter, while here it is the gate voltage.

Some final comments follow. First, because electron transport in graphene is characterized by strong scattering by any lattice defects and both armchair and zigzag edges are equally affected by edge imperfection,[9] it is expected that zigzag GNRs possess a finite transport gap in a geometry with wide leads as explicitly shown in the noninteracting approach in Fig. 3. That is also expected for ribbons with general edges,[18] which are not considered here. Second, the effect due to next-neighbor hopping is not included in above theory. The extended Hückel model with five next-nearest-neighbor hopping energies shows[50] that correction to the nearest-neighbor approximation for the bandgap is small, though other studies[27,51] show that it might be not so. Third, the effects due to the Coulomb interaction on the transport gap in disordered GNRs are a substantial topic that deserves a separate study. Fourth, the Hartree approach used in this study can be combined with the scalable tight-binding model[52] to simulate graphene devices of much larger sizes. Fifth, phonons are known to be the dominant heat carriers in the ungated graphene samples near room temperature.[53] They also affect electron transport for neutral graphene due to considerable electron–phonon coupling.[54] However, in doped graphene, which is a subject of this study, phonon effects are negligible.[53,54]

VI. CONCLUSION

Quantum-mechanical calculations of electron transport in both noninteracting and interacting approaches predict that the semiconductor/metal alternation pattern that is widely discussed in the literature for armchair GNRs is much weaker and inverted for the setup with wide leads. This is a result of the strong electron scattering on the ribbon-to-lead interfaces. The long-range Coulomb electron interactions cause the transport gap to vanish for all widths of GNRs in the straight geometry due to subband pinning to the chemical potential. In geometry with wide leads, the interaction results in additional deviation of the alternation pattern. These findings demonstrate that the transport gaps that are typically discussed in the literature are hardly able to be observed in lithographically patterned graphene ribbons, not only because of defects inside the ribbon but also because of interaction effects and setup geometry.

ACKNOWLEDGMENTS

This work was supported by SNIC (No. 2020/13-95). I thank Philip Kim for comments.

AUTHOR DECLARATIONS

Conflicts of Interest

The author has no conflicts to disclose.

APPENDIX A: LENGTH DEPENDENCE OF TRANSPORT GAP

Figure 7 shows E_{gap} and V_{gap} as a function of ribbon length for fixed width and interface length. The lead width is twice the ribbon width and the gaps are averaged over ten neighbor N_l for the noninteracting and three neighbors for the Hartree approach. The gaps do not depend on the ribbon length because quantization of energy spectrum is defined in the cross-sectional direction. Some fluctuations of E_{gap} are observed due to wave function interference between ribbon entrance and exit points and insufficient averaging at $T = 0$. The results for the Hartree approach are obtained for $T = 100$ K so temperature acts additionally as an averaging quantity. Independence of the transport gap on ribbon length agrees with previous studies.[2,3,9]

APPENDIX B: HARTREE POTENTIAL

In this appendix, representative distribution of Hartree potential V_H, Eq. (5), is discussed. Figure 8 shows V_H at the interface between the left-hand lead and GNR. The magnitude of $\mu - V_H$ raises near the edges, which indicates charge accumulation along the boundaries.[24,25] The potential fluctuations of the order of $0.1t$, which are generated, e.g., by the charged impurities, should affect

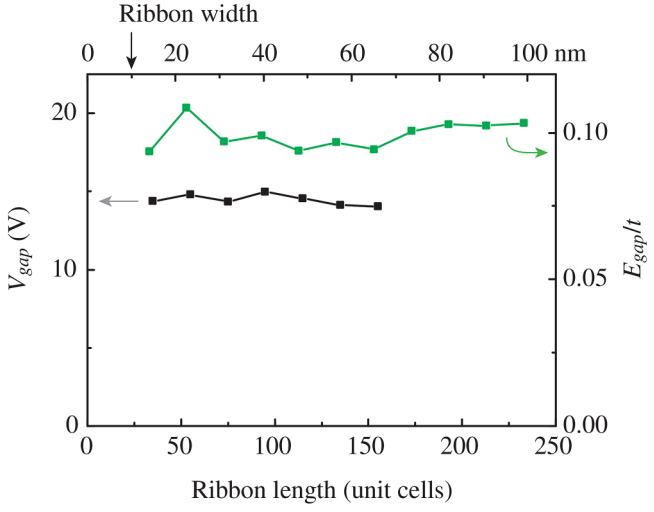

FIG. 7. Transport gap in the noninteracting (right axis) and Hartree (left axis) approaches as a function of ribbon length. $N = 80$, $N_l \approx 2N$, and $L = 30$.

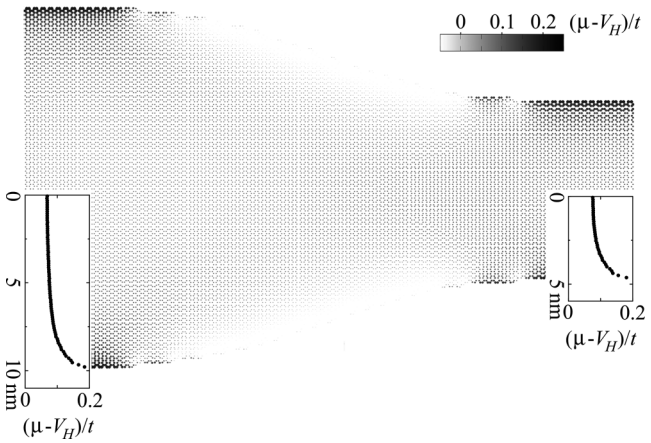

FIG. 8. The Hartree potential V_H, Eq. (5), subtracted from μ, at the conduction edge. The inset panels at the bottom show the profiles in the leads and the ribbon. $N = 80$, $N_l \approx 2N$, and $L = 30$.

the distributions of V_H, n, and thus the transport gap values. The effects of such fluctuations, however, are outside the scope of this study, which is rather devoted to the *ideal* GNRs. The effects due to various disorder types, using the *noninteracting* approach, were previously studied in Refs. 9–12.

DATA AVAILABILITY

The data that support the findings of this study are available from the corresponding author upon reasonable request.

REFERENCES

[1]S. Adam, S. Cho, M. S. Fuhrer, and S. Das Sarma, Phys. Rev. Lett. **101**, 046404 (2008).
[2]P. Gallagher, K. Todd, and D. Goldhaber-Gordon, Phys. Rev. B **81**, 115409 (2010).
[3]M. Y. Han, J. C. Brant, and P. Kim, Phys. Rev. Lett. **104**, 056801 (2010).
[4]J. B. Oostinga, B. Sacépé, M. F. Craciun, and A. F. Morpurgo, Phys. Rev. B **81**, 193408 (2010).
[5]F. Molitor, A. Jacobsen, C. Stampfer, J. Güttinger, T. Ihn, and K. Ensslin, Phys. Rev. B **79**, 075426 (2009).
[6]F. Molitor, C. Stampfer, J. Güttinger, A. Jacobsen, T. Ihn, and K. Ensslin, Semicond. Sci. Technol. **25**, 034002 (2010).
[7]N. J. G. Couto, B. Sacépé, and A. F. Morpurgo, Phys. Rev. Lett. **107**, 225501 (2011).
[8]M. Y. Han, B. Ozyilmaz, Y. Zhang, and P. Kim, Phys. Rev. Lett. **98**, 206805 (2007).
[9]E. R. Mucciolo, A. H. Castro Neto, and C. H. Lewenkopf, Phys. Rev. B **79**, 075407 (2009).
[10]M. Evaldsson, I. V. Zozoulenko, H. Xu, and T. Heinzel, Phys. Rev. B **78**, 161407 (2008).
[11]D. Querlioz, Y. Apertet, A. Valentin, K. Huet, A. Bournel, S. Galdin-Retailleau, and P. Dollfus, Appl. Phys. Lett. **92**, 042108 (2008).
[12]M. Poljak, E. B. Song, M. Wang, T. Sulogoj, and K. L. Wang, IEEE Trans. Electron Devices **59**, 3231 (2012).
[13]V. Saraswat, R. M. Jacobberger, and M. S. Arnold, ACS Nano **15**, 3674 (2021).
[14]D. V. Kosynkin, A. L. Higginbotham, A. Sinitskii, J. R. Lomeda, A. Dimiev, B. K. Price, and J. M. Tour, Nature **458**, 872 (2009); J. Lim, U. N. Maiti, N.-Y. Kim, R. Narayan, W. J. Lee, D. S. Choi, Y. Oh, J. M. Lee, G. Y. Lee, S. H. Kang, H. Kim, Y.-H. Kim, and S. O. Kim, Nat. Commun. **7**, 10364 (2016); Y.-S. Li, J.-L. Liao, S.-Y. Wang, and W.-H. Chiang, Sci. Rep. **6**, 22755 (2016).
[15]J. P. Llinas, A. Fairbrother, G. B. Barin, W. Shi, K. Lee, S. Wu, B. Y. Choi, R. Braganza, J. Lear, N. Kau, W. Choi, C. Chen, Z. Pedramrazi, T. Dumslaff, A. Narita, X. Feng, K. Müllen, F. Fischer, A. Zettl, P. Ruffieux, E. Yablonovitch, M. Crommie, R. Fasel, and J. Bokor, Nat. Commun. **8**, 633 (2017).
[16]V. Saraswat, Y. Yamamoto, H. J. Kim, R. M. Jacobberger, K. R. Jinkins, A. J. Way, N. P. Guisinger, and M. S. Arnold, ECS Trans. **93**, 133 (2019).
[17]K. Tanaka, S. Yamashita, H. Yamabe, and T. Yamabe, Synth. Met. **17**, 143 (1987).
[18]K. Nakada, M. Fujita, G. Dresselhaus, and M. S. Dresselhaus, Phys. Rev. B **54**, 17954 (1996).
[19]L. Brey and H. A. Fertig, Phys. Rev. B **73**, 235411 (2006).
[20]K. Wakabayashi, K. Sasaki, T. Nakanishi, and T. Enoki, Sci. Technol. Adv. Mater. **11**, 054504 (2010).
[21]D. A. Areshkin, D. Gunlycke, and C. T. White, Nano Lett. **7**, 204 (2007); D. Gunlycke, D. A. Areshkin, and C. T. White, Appl. Phys. Lett. **90**, 142104 (2007).
[22]A. H. Castro Neto, F. Guinea, N. M. R. Peres, K. S. Novoselov, and A. K. Geim, Rev. Mod. Phys. **81**, 109 (2009).
[23]The relation between E_{gap} and V_{gap} is derived for 2D graphene in a parallel plate capacitor setup and assuming that it holds true at the onset of the first quantization step in nanoribbon geometry.
[24]J. Fernández-Rossier, J. J. Palacios, and L. Brey, Phys. Rev. B **75**, 205441 (2007).
[25]A. A. Shylau, J. W. Kłos, and I. V. Zozoulenko, Phys. Rev. B **80**, 205402 (2009).
[26]Y.-W. Son, M. L. Cohen, and S. G. Louie, Phys. Rev. Lett. **97**, 216803 (2006).
[27]C. T. White, J. Li, D. Gunlycke, and J. W. Mintmire, Nano Lett. **7**, 825 (2007).
[28]J. Davies, *The Physics of Low-Dimensional Semiconductors* (Cambridge University Press, Cambridge, 1998).
[29]P. G. Silvestrov and K. B. Efetov, Phys. Rev. B **77**, 155436 (2008).
[30]S. Ihnatsenka and G. Kirczenow, Phys. Rev. B **86**, 075448 (2012).
[31]I. J. Vera-Marun, P. J. Zomer, A. Veligura, M. H. D. Guimaraës, L. Visser, N. Tombros, H. J. van Elferen, U. Zeitler, and B. J. van Wees, Appl. Phys. Lett. **102**, 013106 (2013).
[32]D. A. Areshkin and B. K. Nikolić, Phys. Rev. B **81**, 155450 (2010).
[33]S. Datta, *Electronic Transport in Mesoscopic Systems* (Cambridge University Press, Cambridge, 1997).
[34]S.-H. Ke, H. U. Baranger, and W. Yang, Phys. Rev. B **70**, 085410 (2004).
[35]H. Xu, T. Heinzel, M. Evaldsson, and I. V. Zozoulenko, Phys. Rev. B **77**, 245401 (2008).
[36]C. Caroli, R. Combescot, P. Nozieres, and D. Saint-James, J. Phys. C: Solid State Phys. **4**, 916 (1971).
[37]S. Ihnatsenka, I. V. Zozoulenko, and M. Willander, Phys. Rev. B **75**, 235307 (2007).
[38]K. Wakabayashi, Phys. Rev. B **64**, 125428 (2001).
[39]F. Muñoz-Rojas, D. Jacob, J. Fernández-Rossier, and J. J. Palacios, Phys. Rev. B **74**, 195417 (2006).
[40]J. Wurm, M. Wimmer, I. Adagideli, K. Richter, and H. U. Baranger, New J. Phys. **11**, 095022 (2009).
[41]F. Libisch, A. Kliman, S. Rotter, and J. Burgdörfer, Phys. Status Solidi B **253**, 2366 (2016); F. Libisch, S. Rotter, and J. Burgdörfer, arXiv:1102.3848v1.
[42]V_{gap} definition adopted is this work allows a simple condition in computer code and easy analysis of large datasets. Another definition used in the literature (Refs. 2, 3, 5, and 6) identifies V_{gap} by extrapolating dG/dV_g to zero and if adopted for data in Fig. 5(a) gives 0.12 V, which is about seven times smaller than the value shown in Fig. 5(a). In practical electric circuits, $V_{gap}/2$ might play the role of a threshold voltage similar to the base-to-emitter voltage in a silicon transistor.
[43]D. B. Chklovskii, B. I. Shklovskii, and L. I. Glazman, Phys. Rev. B **46**, 4026 (1992).

[44]E. Ahlswede, P. Weitz, J. Weis, K. von Klitzing, and K. Eberl, Physica B **298**, 562 (2001).
[45]N. Merino-Diez, A. Garcia-Lekue, E. Carbonell-Sanroma, J. Li, M. Corso, L. Colazzo, F. Sedona, D. Sámchez-Portal, J. Pascual, and D. G. de Oteyza, ACS Nano **11**, 11661 (2017).
[46]T. Enoki, Y. Kobayashi, and K.-I. Fukui, Int. Rev. Phys. Chem. **26**, 609 (2007).
[47]S. Ihnatsenka and I. V. Zozoulenko, Phys. Rev. B **79**, 235313 (2009).
[48]N. Nemec, D. Tomànek, and G. Cuniberti, Phys. Rev. B **77**, 125420 (2008).
[49]M. Poljak and M. Matič, Materials **14**, 3670 (2021).
[50]H. Raza and E. C. Kan, Phys. Rev. B **77**, 245434 (2008).
[51]D. Gunlycke and C. T. White, Phys. Rev. B **77**, 115116 (2008); Y. Hancock, A. Uppstu, K. Saloriutta, A. Harju, and M. J. Puska, *ibid* **81**, 245402 (2010).
[52]M.-H. Liu, P. Rickhaus, P. Makk, E. Tóvári, R. Maurand, F. Tkatschenko, M. Weiss, Ch. Schönenberger, and K. Richter, Phys. Rev. B **114**, 036601 (2015).
[53]D. L. Nika and A. A. Balandin, Rep. Prog. Phys. **80**, 036502 (2017).
[54]Th. Sohier, M. Calandra, and F. Mauri, Phys. Rev. B **96**, 075448 (2017).